Magnetoelastic coupling in multiferroic $Ni_3V_2O_8$

L. I. Vergara,[1] J. Cao,[1] N. Rogado,[2] Y. Q. Wang,[3] R. P. Chaudhury,[3] R. J. Cava,[2] B. Lorenz,[3] and J. L. Musfeldt[1]
[1]*Department of Chemistry, University of Tennessee, Knoxville, Tennessee 37996, USA*
[2]*Department of Chemistry and Princeton Materials Institute, Princeton University, Princeton, New Jersey 08544, USA*
[3]*Department of Physics and TCSUH, University of Houston, Houston, Texas 77204, USA*
(Received 5 May 2009; revised manuscript received 20 July 2009; published 27 August 2009)

We measured the infrared-active vibrational modes of the Kagomé staircase compound $Ni_3V_2O_8$ as a function of temperature to elucidate magnetoelastic interactions and local structure changes through the series of magnetic-ordering transitions. A detailed analysis of frequency-shift trends demonstrates that the phonons are sensitive to different magnetic states, indicating that the lattice is flexible and coupled to the spin system. Combining this data with an analysis of displacement patterns, we discuss the local distortions in the ferroelectric phase.

DOI: 10.1103/PhysRevB.80.052303 PACS number(s): 75.50.−y, 33.20.Tp, 63.20.−e, 75.30.Et

Control of the coupling between polarization and magnetization in multiferroic materials is of great current interest, providing opportunities for both fundamental mechanistic advancement and device applications.[1–6] As with other complex oxides, this coupling is mediated by the delicate interplay between magnetism, structure, and charge. Magnetostriction is central to this process,[7–13] although the specific nature of correlations between ferroelectricity, magnetic order, and the lattice (especially the microscopic aspects of structural distortions) remains an open question. Local bond length and angle modifications are made manifest in the dynamics,[14–16] and normal-mode frequency shifts, although subtle, have direct connections to local structure distortions and spin-phonon coupling constants.[17–20] In this work, we exploit the sensitivity of vibrational spectroscopy to establish connections between the lattice dynamics and magnetic states in a magnetically driven multiferroic.

$Ni_3V_2O_8$ displays an orthorhombic (*Cmca*) structure, with layers of edge sharing NiO_6 octahedra separated by nonmagnetic VO_4 tetrahedra.[21] The Ni^{2+} ($S=1$) centers reside in two distinctly different local symmetry environments: "spine" and "crosstie" sites abbreviated here as Ni_s and Ni_c. The spine sites form chains that run along the *a* axis. The chains are connected in the *c* direction by the crosstie sites. Buckling of the quasi-Kagomé planes gives rise to high degree of magnetic anisotropy and leads to a complex magnetic-temperature (*H-T*) phase diagram.[22–25] The latter is characterized by a series of magnetic phase transitions with decreasing temperature. $Ni_3V_2O_8$ is paramagnetic (PM) above 9.8 K. Two incommensurate phases are observed at lower temperatures. The high-temperature incommensurate (HTI) phase displays a collinear sinusoidal modulation whereas the low-temperature incommensurate (LTI) phase has a spiral spin structure.[23] The latter is ferroelectric with spontaneous polarization along *b* ($P_b \sim 100\ \mu C/m^2$). Below the LTI phase, commensurate canted antiferromagnetism is observed. In recent dilatometry experiments,[26] small anomalies in the lattice parameters were detected when crossing the PM $\rightarrow$HTI transition at 9.8 K and HTI$\rightarrow$LTI at 6.5 K. The dielectric constant along *b* displays a peak at the HTI$\rightarrow$LTI transition and a small drop in the LTI phase.[27]

In order to elucidate magnetic-ordering-induced lattice distortions and spin-lattice coupling in a magnetically driven multiferroic, we investigated the infrared response of $Ni_3V_2O_8$ as a function of temperature. Magnetoelastic coupling is evidenced by vibrational frequency shifts at different magnetic-ordering temperatures. From a detailed analysis of the mode trends, displacement patterns,[13,28] and dilatometry results,[26] we elucidate and discuss local structure changes in the different magnetic phases. We also discuss magnetoelectric coupling in the low-temperature multiferroic phase in light of recent theoretical predictions.[13,28]

$Ni_3V_2O_8$ single crystals were grown as described earlier.[25,26] Near normal reflectance was measured on both the as-grown *ac* plane and on cut crystals exposing the *b* axis. Although we employed a series of spectrometers,[25] the majority of work was done using a Bruker 113V Fourier transform infrared spectrometer with bolometer detector, covering the 20–5000 cm^{-1} frequency range with 0.5 cm^{-1} resolution.[29] Polarizers were employed to select the *a*, *b*, and *c* directions.[30] For variable-temperature studies, we used an open-flow helium cryostat equipped with a temperature controller. Optical conductivity, σ_1, and dielectric constant, ϵ_1, were calculated by a Kramers-Kronig analysis.[31]

Figure 1 displays the 300 K polarized optical conductivity of $Ni_3V_2O_8$. The spectra are characteristic of an anisotropic material, with vibrational excitations that are strongly dependent on the polarization direction. Peak assignments were carried out based upon existing first-principles calculations[13,28] and are tabulated in Ref. 28. We relied on these identifications to label the modes and the purpose of the present report is to study the temperature dependence of these modes through the series of magnetic-ordering (and electric-ordering) transitions. The spectra consist of two well-separated frequency regimes. The low-frequency regime (120–500 cm^{-1}) contains the rigid motion of the NiO_6 octahedra and VO_4 tetrahedra plus O-V-O and O-Ni-O bending, causing small polyhedral distortions. The high-frequency regime (500–900 cm^{-1}) involves mainly O atom vibrations along the V-O bonds. Since all oxygen atoms are connected to Ni atoms, these modes cannot be described as purely V-O stretching modes because they are always mixed with some Ni-O bond stretching or O-Ni-O bending. Displacement pattern animations are available in Ref. 32.

The temperature dependence of the infrared-active phonons provides specific information about lattice contrac-

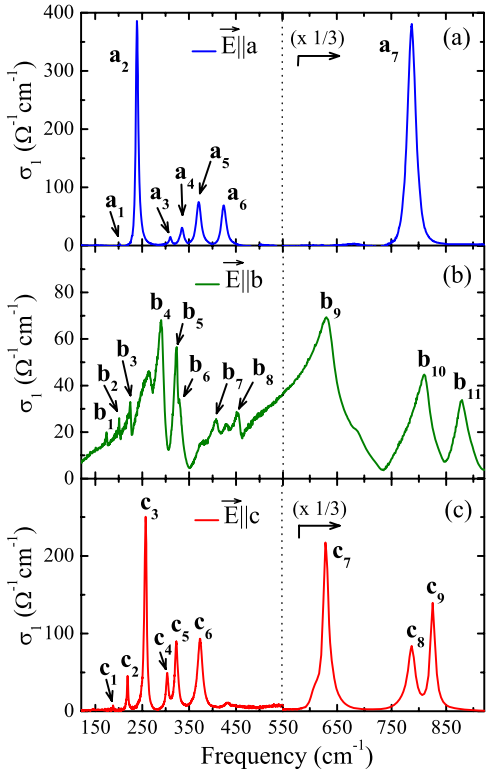

FIG. 1. (Color online) 300 K optical conductivity of $Ni_3V_2O_8$ along the *a*, *b*, and *c* directions. Mode intensities above 550 cm^{-1} were reduced by a factor of 3 in panels (a) and (c) for clarity.

tion. Initially, all modes harden with decreasing temperature. For most features, the temperature dependence of the mode frequency is well described as $\omega_j = \omega_{0,j}\{1 - c_j/[\exp(\Theta/T) - 1]\}$, where $\omega_{0,j}$ indicates the frequency of the *j*th mode in absence of spin-phonon coupling at 0 K, c_j is a mode-dependent anharmonic scaling factor, and Θ is the Debye temperature (600 K).[33,34] Between 50 and 100 K, several modes reveal significant deviations from anharmonic behavior, with the strongest effects along the spine direction. Anomalous phonon shifts, taking place at much higher temperature than the magnetic-ordering transition temperature, have been reported for other multiferroics,[35–38] although here, it seems to be a precursor effect or spin-phonon coupling rather than evidence for a new energy scale. Since Θ_{CW} is on the order of −30 K, it is reasonable to expect short-range spin correlations to develop in this temperature range.

In order to distinguish the natural anharmonic contribution from more subtle temperature effects that occur as $Ni_3V_2O_8$ is tuned through the series of magnetic-ordering transitions, we analyze frequency shifts of the modes in the low-temperature range (Fig. 2). One way to analyze these shifts is via comparison of peak positions at consecutive temperatures: $\Delta\omega/\omega = [\omega(T_{low}) - \omega(T_{high})]/\omega(T_{low})$. A positive difference indicates that the mode in question is hardening across the magnetic phase boundary. A negative difference indicates that the mode is softening or relaxing. Over the small temperature intervals studied here, no substantial anharmonic contribution is anticipated. Thus, observed mode softening or hardening demonstrates lattice sensitivity to the magnetic state. Of course, these measured frequency shifts

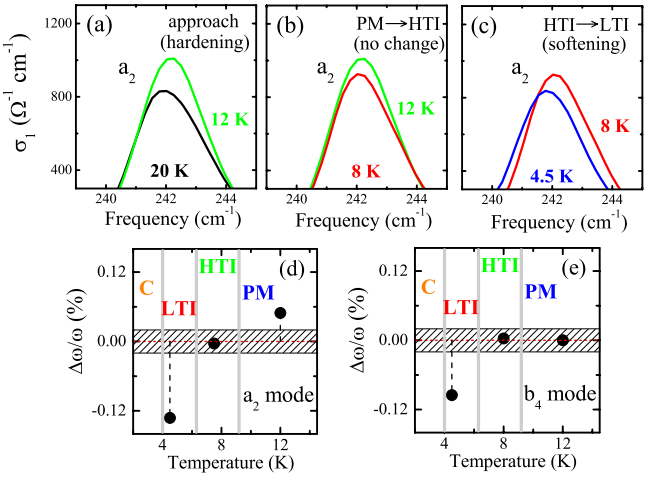

FIG. 2. (Color online) Close-up view of the a_2 mode measured (a) on approach to the series of magnetic transitions, (b) across the PM to HTI boundary, and (c) through the HTI to LTI transition. The intensity changes are typical. [(d) and (e)] Relative frequency change for a_2 and b_4 modes, respectively. The shaded area with $|\Delta\omega/\omega| \leq 0.02\%$ displays our sensitivity limit determined via peak-fit techniques and visual confirmation.

capture both local lattice distortions and changes in spin-phonon coupling constants. Both are discussed below, although emphasis is placed on analysis of local distortions. In $Ni_3V_2O_8$, the observed frequency shifts are on the order of 0.03–0.12 %. Shifts in RMn_2O_5 (R=rare earth) and other materials are also small.[17,36–38]

We perform this frequency-shift analysis on all observed *a*-, *b*-, and *c*-polarized vibrational modes, focusing on three stages of the cooling process: (i) the approach to the series of magnetic transitions, (ii) the PM to HTI phase transition, and (iii) the HTI to ferroelectric LTI transition. We compare spectra at 20, 12, 8, and 4.5 K, temperatures selected to be at the heart of each magnetic phase. Our detailed trends are summarized in Table I. Numerical values for the frequency shifts are given in the electronic auxiliary material.[39]

On approach to the series of magnetic-ordering transitions (between 20 and 12 K), the high-frequency modes $\mathbf{a}_7$, b_{11}, and b_9, soften. Here, bold designates modes with largest frequency shifts. These modes involve large oxygen center displacements, mainly due to VO_4 stretching. All low-frequency modes along the crosstie direction ($\mathbf{c}_6$, $\mathbf{c}_5$, c_4, $\mathbf{c}_3$, and c_2) harden. Hardening of b_6, $\mathbf{b}_1$, and a_2 is also observed. Together, these modes involve $(a+c)$-directed motion of Ni_s and $(c+b)$-directed motion of Ni_c. This response is a pretransitional effect, which we attribute to large amplitude Ni_s-O-Ni_s and Ni_s-O-Ni_c superexchange fluctuations and formation of short-range order. These short-range spin correlations are due to frustration and become more cohesive on approach to the series of magnetic-ordering transitions.

The PM to HTI transition involves hardening of $\mathbf{a}_7$ and c_7, plus softening of c_6, c_5, c_4, c_3, c_2, and b_5. With an 0.13% frequency shift, $\mathbf{a}_7$ is the most important displacement and involves substantial oxygen motion driven by VO_4 stretching, with consequent modification of the Ni_s-O-Ni_c angle and associated superexchange. If we broaden our criteria and

TABLE I. (Color online) Summary of the vibrational trends through the series of magnetic-ordering transitions in $Ni_3V_2O_8$. Peak-fitting techniques and visual confirmation were used to establish these trends. Hardening or softening indicates $|\Delta\omega/\omega| \geq 0.02\%$.

Magnetic-ordering transitions of interest	$\vec{E}\|a$ High frequency	$\vec{E}\|a$ Low frequency					$\vec{E}\|b$ High frequency			$\vec{E}\|b$ Low frequency						$\vec{E}\|c$ High frequency			$\vec{E}\|c$ Low frequency					Frequency Shifts
	a_7	a_6	a_5	a_4	a_3	a_2	b_{11}	b_{10}	b_9	b_6	b_5	b_4	b_3	b_2	b_1	c_9	c_8	c_7	c_6	c_5	c_4	c_3	c_2	
Short-range fluctuations: Approaching the series of magnetic transitions						●				●					●				●	●	●	●	●	hardening
		●	●	●	●			●			●	●	●	●		●	●	●						no change
	●						●		●															softening
PM → HTI	●																	●						hardening
		●	●	●	●	●	●	●	●	●		●	●	●	●	●	●							no change
											●								●	●	●	●	●	softening
HTI → LTI										●	●												●	hardening
							●		●				●	●	●	●	●		●	●	●			no change
	●	●	●	●	●	●		●				●												softening

consider modes that undergo medium-sized frequency changes (0.06–0.08 %), we find that there are a number of transverse relaxations (c_6, c_5, c_3, c_2, and b_5) that counteract the aforementioned spine-directed contraction. Ni_c motion is observed for the majority of these features; c_2, which involves shearing of Ni_c along c, is especially clear. In contrast, Ni_s displacement is observed only in c_3. Taken together, the behavior of these features indicates transverse local lattice distortions involving Ni centers, with displacements mostly along c (and to a much lesser extent, along b) [Fig. 3(a)] that distort the NiO_6 octahedra and induce changes in the Ni-O-Ni angles. We conclude that local lattice distortions that change the Ni_s-O-Ni_c superexchange interaction are most important here.

The HTI to LTI transition is complex and involves several modes. All spine-directed modes $\mathbf{a}_7$, a_6, a_5, a_4, a_3, and $\mathbf{a}_2$, plus b_{10}, $\mathbf{b}_4$, and c_7, soften. b_6, b_5, c_3, and c_2 harden. To identify the most important local lattice distortions, we group

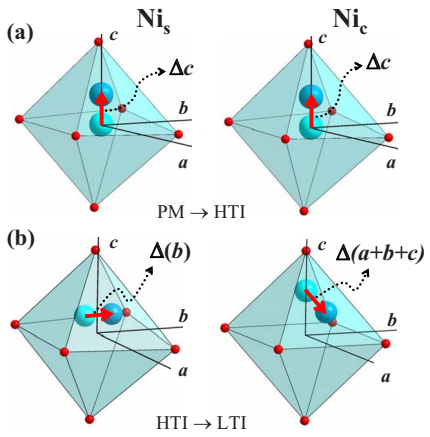

FIG. 3. (Color online) Schematic representation of Ni displacements in $Ni_3V_2O_8$ (a) across the PM to HTI boundary and (b) through the HTI to LTI transition, determined by vibrational measurements and analysis of displacement vectors. Aqua and teal atoms represent the initial and displaced position of the Ni center. O centers are static for clarity in this rendering.

the modes based upon the magnitude of the frequency shift across the HTI→LTI boundary. We find $\mathbf{a}_2$, $\mathbf{b}_4$, and $\mathbf{a}_7$ to be the most relevant. The high-frequency $\mathbf{a}_7$ mode involves large oxygen displacements along the spine direction due to the VO_4 asymmetric stretch. $\mathbf{b}_4$ and $\mathbf{a}_2$ show significant Ni center displacements, with frequency shifts on the order of 0.10% and 0.13%, respectively. $\mathbf{b}_4$ involves Ni_s motion along b plus diagonal Ni_c motion along b and c. This is the mode that breaks inversion symmetry. $\mathbf{a}_2$ involves Ni_c motion along a and a slight (almost negligible) displacement of Ni_s along c. Combining these results, Ni_s displaces mainly along b, perpendicular to the chain, whereas Ni_c moves along a, b, and c [Fig. 3(b)]. Oxygen motion accommodates the strong Ni displacements mandated by $\mathbf{b}_4$ and $\mathbf{a}_2$. We can test this conclusion by relaxing our criteria to include b_5, a_6, a_5, and c_3 in the analysis. These modes display more modest frequency shifts (between 0.06% and 0.08%). b_5 and a_6 indicate $(a+b+c)$-directed Ni_c motion, a result that reinforces that extracted from analysis of $\mathbf{a}_2$ and $\mathbf{b}_4$ alone. The remaining modes involve oxygen motion driven by bending and tilting of the VO_4 tetrahedra, without substantial Ni displacements. The Ni_s and Ni_c shifts cause significant modification of the Ni_s-O-Ni_c superexchange interactions (and, to a much lesser extent, the Ni_s-O-Ni_s superexchange). These local lattice distortions point toward a slight compression of the octahedra in the ferroelectric phase, in line with the overall b-axis expansion and c-axis contraction found in dilatometry studies.[26] Extrapolating our dielectric constant data to zero frequency, we estimate $\Delta\epsilon_1(0) \approx 1-2$ % along a, b, and c, in reasonable agreement with static dielectric constant data.[27]

Recent theoretical work predicted $\mathbf{b}_4$ to be one of the most important modes for establishing the b-directed spontaneous polarization in the LTI phase.[13,23,28] Our finding that $\mathbf{b}_4$ softens considerably at this transition (i) is consistent with theory, (ii) demonstrates the symmetry breaking needed to establish ferroelectricity, and (iii) is in line with the expectation that the softest phonons contribute most to the polarization. That the $\mathbf{a}_2$ and $\mathbf{a}_7$ modes also participate in the HTI →LTI transition indicates a more complex local lattice distortion than originally anticipated and opens the door to con-

sideration of new mechanisms for spin-phonon coupling. A comprehensive model to estimate spin-phonon coupling constants (λ) in the PM phase and across the series of magnetic transitions is under development. Early estimates indicate λ's up to ≈ 500 meV/Å^2, depending on the mode.

Summarizing, we employed vibrational spectroscopy to investigate magnetoelastic coupling through the series of low-temperature magnetic-ordering transitions in $Ni_3V_2O_8$, a magnetically driven multiferroic. The transition to the ferroelectric low-temperature incommensurate phase takes place with $\mathbf{b}_4$, $\mathbf{a}_2$, and $\mathbf{a}_7$ mode frequency shifts that we analyze in terms of local distortion of both Ni_s and Ni_c centers. The contribution of $\mathbf{b}_4$ to the finite polarization was anticipated by symmetry arguments. That local structure is sensitive to the magnetic state has important consequences for other functional oxides where many exotic properties derive from the interplay between structure and magnetism.

This work is supported by the Department of Energy (UT, Princeton) and the State of Texas (TCSUH). We thank A.B. Harris, M. Kenzelmann, G. Lawes, A.B. Sushkov, and T. Yildirim for useful discussions.

[1] S. Matsumoto *et al.*, Ferroelectrics **286**, 185 (2003).
[2] L. C. Chapon, G. R. Blake, M. J. Gutmann, S. Park, N. Hur, P. G. Radaelli, and S. W. Cheong, Phys. Rev. Lett. **93**, 177402 (2004).
[3] N. Hur, S. Park, P. A. Sharma, S. Guha, and S. W. Cheong, Phys. Rev. Lett. **93**, 107207 (2004).
[4] B. Mihailova, M. M. Gospodinov, B. Guttler, F. Yen, A. P. Litvinchuk, and M. N. Iliev, Phys. Rev. B **71**, 172301 (2005).
[5] N. Hur *et al.*, Nature (London) **429**, 392 (2004).
[6] D. Higashiyama, S. Miyasaka, N. Kida, T. Arima, and Y. Tokura, Phys. Rev. B **70**, 174405 (2004).
[7] Y. Boonyongmaneerat, M. Chmielus, D. C. Dunand, and P. Mullner, Phys. Rev. Lett. **99**, 247201 (2007).
[8] C. R. dela Cruz, B. Lorenz, Y. Y. Sun, C. W. Chu, S. Park, and S. W. Cheong, Phys. Rev. B **74**, 180402(R) (2006).
[9] B. García-Landa, C. Marquina, M. R. Ibarra, G. Balakrishnan, M. R. Lees, and D. M. Paul, Phys. Rev. Lett. **84**, 995 (2000).
[10] A. N. Lavrov, S. Komiya, and Y. Ando, Nature (London) **418**, 385 (2002).
[11] S. E. Russek *et al.*, J. Appl. Phys. **91**, 8659 (2002).
[12] V. S. Zapf *et al.*, Phys. Rev. B **77**, 020404(R) (2008).
[13] A. B. Harris, T. Yildirim, A. Aharony, and O. Entin-Wohlman, Phys. Rev. B **73**, 184433 (2006).
[14] T. Ruf, C. Thomsen, R. Liu, and M. Cardona, Phys. Rev. B **38**, 11985 (1988).
[15] M. Rini *et al.*, Nature (London) **449**, 72 (2007).
[16] A. B. Sushkov, J. L. Musfeldt, Y. J. Wang, R. M. Achey, and N. S. Dalal, Phys. Rev. B **66**, 144430 (2002).
[17] W. Baltensperger and J. S. Helman, Helv. Phys. Acta **41**, 668 (1968).
[18] S. Picozzi, K. Yamauchi, G. Bihlmayer, and S. Blugel, Phys. Rev. B **74**, 094402 (2006).
[19] C. Wang, G. C. Guo, and L. He, Phys. Rev. Lett. **99**, 177202 (2007).
[20] C. J. Fennie and K. M. Rabe, Phys. Rev. Lett. **96**, 205505 (2006).
[21] E. E. Sauerbrei, R. Faggiani, and C. Calvo, Acta Crystallogr., Sect. B: Struct. Crystallogr. Cryst. Chem. **29**, 2304 (1973).
[22] G. Lawes *et al.*, Phys. Rev. Lett. **93**, 247201 (2004).
[23] G. Lawes *et al.*, Phys. Rev. Lett. **95**, 087205 (2005).
[24] M. Kenzelmann *et al.*, Phys. Rev. B **74**, 014429 (2006).
[25] R. C. Rai, J. Cao, S. Brown, J. L. Musfeldt, D. Kasinathan, D. J. Singh, G. Lawes, N. Rogado, R. J. Cava, and X. Wei, Phys. Rev. B **74**, 235101 (2006).
[26] R. P. Chaudhury, F. Yen, C. R. dela Cruz, B. Lorenz, Y. Q. Wang, Y. Y. Sun, and C. W. Chu, Phys. Rev. B **75**, 012407 (2007).
[27] G. Lawes *et al.*, Proceedings of the 12th US-Japan Seminar on Dielectric and Piezoelectric Ceramics, 2005 (unpublished), p. 215.
[28] T. Yildirim *et al.*, J. Phys.: Condens. Matter **20**, 434214 (2008).
[29] This yields 5 data points/cm^{-1}. Our reported peak shifts take advantage of systematic shifts in many such data points through peak-fit techniques (Fig. 2).
[30] For the cut crystal exposing the *b* axis, surface quality issues broadened phonon line widths and caused slight "leakage" of *a* and *c* related features into the spectrum. We also elected not to polish the crystal to avoid damage or polishing-induced stress. Despite these challenges, *b*-polarized phonon positions are highly reliable. Additional oscillators were, however, required to capture peak widths and asymmetries and get acceptable fits to the line shapes. Overall, the *b*-polarized data showed remarkably good agreement with the dynamics calculations of Ref. 28. Only one experimental peak (between b_3 and b_4) remains unassigned.
[31] F. Wooten, *Optical Properties of Solids* (Academic, New York, 1972).
[32] Animations of the B_{2u} phonons can be found at http://www.ncnr.nist.gov/staff/taner/nvo
[33] T. Rudolf, C. Kant, F. Mayr, J. Hemberger, V. Tsurkan, and A. Loidl, Phys. Rev. B **75**, 052410 (2007).
[34] R. C. Rai, J. Cao, L. I. Vergara, S. Brown, J. L. Musfeldt, D. J. Singh, G. Lawes, N. Rogado, R. J. Cava, and X. Wei, Phys. Rev. B **76**, 174414 (2007).
[35] A. B. Sushkov, O. Tchernyshyov, W. Ratcliff, S. W. Cheong, and H. D. Drew, Phys. Rev. Lett. **94**, 137202 (2005).
[36] A. F. García-Flores, E. Granado, H. Martinho, R. R. Urbano, C. Rettori, E. I. Golovenchits, V. A. Sanina, S. B. Oseroff, S. Park, and S. W. Cheong, Phys. Rev. B **73**, 104411 (2006).
[37] J. Cao, L. I. Vergara, J. L. Musfeldt, A. P. Litvinchuk, Y. J. Wang, S. Park, and S. W. Cheong, Phys. Rev. Lett. **100**, 177205 (2008).
[38] J. Cao, L. I. Vergara, J. L. Musfeldt, A. P. Litvinchuk, Y. J. Wang, S. Park, and S. W. Cheong, Phys. Rev. B **78**, 064307 (2008).
[39] See EPAPS Document No. E-PRBMDO-80-023929 for the numerical values for the frequency shifts. For more information on EPAPS, see http://www.aip.org/pubservs/epaps.html.